ON ANGULAR-DOMAIN CHANNEL ESTIMATION FOR ONE-BIT MASSIVE MIMO SYSTEMS WITH FIXED AND TIME-VARYING THRESHOLDS

Pu Wang[1]*, Jian Li*[2*]*, Milutin Pajovic*[1]*, Petros T. Boufounos*[1]*, and Philip V. Orlik*[1]

[1] Mitsubishi Electric Research Laboratories (MERL), Cambridge, MA 02139, USA
E-mails: {pwang, pajovic, petrosb, porlik}@merl.com
[2] University of Florida, Gainesville, Florida 32611, USA
E-mail: li@dsp.ufl.edu.

ABSTRACT

This paper considers angular-domain channel estimation for massive MIMO systems with one-bit analog-to-digital converters (ADCs) equipped at base stations for the sake of lower power consumption and reduced hardware cost. We characterize analytical performance, in terms of the Cramér-Rao bound (CRB), on estimating the two-dimensional channel matrix (including angle-of-departure, angle-of-arrival and associated channel path gains) in the angular-domain representation. Our analysis provides a simple tool to compare the channel estimation performance among several one-bit quantization schemes. Particularly, we study the performance trade-off between fixed (zero-threshold) and time-varying one-bit quantization schemes. Numerical results are provided for analytical performance verification as a function of SNR and the number of pilots.

1. INTRODUCTION

Leveraging a large number of base station antennas to support many single-/multiple-antenna users, massive multiple-input multiple-output (MIMO) systems can significantly increase the spectral efficiency and average out the channel noise and fading [1–3]. More specifically, massive MIMO systems can mitigate propagation loss by exploiting large array gain due to coherent beamforming/combining, reduce interference-leakage as channel estimation errors vanish asymptotically in the large-dimensional vector space, simplify signal processing algorithms, and reduce inter-user interference with the high beamforming resolution.

Despite all these benefits, massive MIMO systems pose new challenges for system design and hardware implementation. For example, the hardware cost and power consumption become prohibitively high as the number of antennas is large and high-resolution analog-to-digital convertors (ADCs) are employed. Those challenges become more severe when the system operates at the millimeter-wave (mmWave) frequency band to exploit the large bandwidth [4–7]. Coined as mmWave massive MIMO systems [8, 9], a large number of antennas must be used for the array gain and link margin to compensate for significant path loss due to the high attenuation and absorption at the mmWave band.

To meet these challenges, several transceiver architectures have been proposed for massive MIMO signal processing, including precoding, combining and channel estimation. An *analog* architecture relies on the RF-domain processing to reduce the number of RF chains. By changing relative phases of the signals, they use a network of analog phase shifters to steer the transmit/receive beams in the desired directions [10, 11]. Potential issues of the analog architecture include the coarse quantization levels of the phase shifting angles, the aging of analog components, and the support of only a single-stream MIMO transmission. A *hybrid analog/digital* architecture can reduce the number of RF chains by combining sub-arrays of antennas with switches, phase shifters and lenses, followed by the digital sampling of the combined signals [12–14]. With more degrees of freedom, a hybrid precoder can support multi-stream and multi-user transmission, while keeping the system cost, complexity, and power consumption low. The third option is a *fully digital* architecture with low-resolution ADCs. Extensive studies have considered channel estimation and symbol detection for massive MIMO systems with low-resolution ADCs (e.g. 1-3 bits) [15–21].

In this paper, we are interested in characterizing the analytical performance of massive MIMO channel estimation when only one-bit ADCs are used. Particularly, we derive the Cramér-Rao bound (CRB) on estimating the angular-domain channel parameters including angle-of-departure (AoD), angle-of-arrival (AoA), and associated channel path gains. Our analysis provides a simple tool to compare the channel estimation performance among several one-bit quantization schemes. Moreover, it reflects, with a fixed threshold at zero, the ambiguity between the channel path gain and the noise variance as the complete Fisher information matrix (FIM) becomes singular. Meanwhile, this ambiguity can be removed if the one-bit ADC uses a time-varying threshold quantization scheme.

The rest of the paper is organized as follows. Section 2 introduces the massive MIMO system model for channel estimation. Section 3 specifies the signal model of one-bit channel measurements. The CRB expressions are derived in Section 4 with known and unknown noise variances. Numerical results are provided in Section 5, followed by concluding remarks in Section 6.

2. MASSIVE MIMO CHANNEL MODEL

Consider a point-to-point uplink massive MIMO system in Fig. 1, with N_t antennas at the mobile station (MS) and N_r antennas at a base station (BS). At time instant k, the MS transmits pilot signals $\mathbf{s}_k \in \mathbb{C}^{N_t \times 1}$ with a normalized transmitting power. At the BS, the received signal $\mathbf{y}_k \in \mathbb{C}^{N_r \times 1}$ is

$$\mathbf{y}_k = \mathbf{H}\mathbf{s}_k + \mathbf{v}_k, \quad k = 1, 2, \cdots, K, \tag{1}$$

where $\mathbf{H} \in \mathcal{C}^{N_r \times N_t}$ is the complex channel matrix, and $\mathbf{v}_k$ is white Gaussian noise with variance σ^2, and K is the number of pilots.

The channel matrix $\mathbf{H}$ in (1) can be represented by a geometric channel model with N_s scatterers between the BS and the MS.

*The work was performed when J. Li was a consultant to MERL.

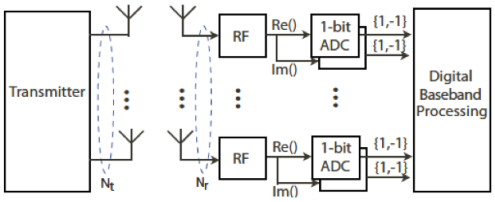

Fig. 1. The massive MIMO system with one-bit ADCs (from [22]).

Specifically,

$$\mathbf{H} = \sum_{i=1}^{N_s} \alpha_i \boldsymbol{\alpha}_{\text{BS}}(\theta_i)\boldsymbol{\alpha}_{\text{MS}}^H(\phi_i) \tag{2}$$

where α_i is the complex path gain associated with the i-th geometric channel path characterized by the AoA θ_i and AoD ϕ_i, respectively. $\boldsymbol{\alpha}_{\text{BS}}(\theta_i)$ and $\boldsymbol{\alpha}_{\text{MS}}(\phi_i)$ denote, respectively, the receiving and transmitting array response vectors. In the case of a uniform linear array (ULA), the array response vectors can be written as $\boldsymbol{\alpha}_{\text{BS}}(\theta) = [1, e^{j2\pi d_r \sin(\theta)/\lambda}, \cdots, e^{j(N_r-1)2\pi d_r \sin(\theta)/\lambda}]^T/\sqrt{N_r}$, and $\boldsymbol{\alpha}_{\text{MS}}(\phi) = [1, e^{j2\pi d_t \sin(\phi)/\lambda}, \cdots, e^{j(N_t-1)2\pi d_t \sin(\phi)/\lambda}]^T/\sqrt{N_t}$ where d_r and d_t denote, respectively, the inter-element spacings of the receiving array at the BS and the transmitting array at the MS, and λ is the wavelength. (2) can be rewritten as

$$\mathbf{H} = \mathbf{A}_{\text{BS}}(\boldsymbol{\theta})\mathbf{H}_a\mathbf{A}_{\text{MS}}^H(\boldsymbol{\phi}) \tag{3}$$

where $\mathbf{A}_{\text{BS}}(\boldsymbol{\theta}) = [\boldsymbol{\alpha}_{\text{BS}}(\theta_1), \cdots, \boldsymbol{\alpha}_{\text{BS}}(\theta_{N_s})]$, $\mathbf{A}_{\text{MS}}(\boldsymbol{\phi}) = [\boldsymbol{\alpha}_{\text{MS}}(\phi_1), \cdots, \boldsymbol{\alpha}_{\text{MS}}(\phi_{N_s})]$, and $\mathbf{H}_a = \text{diag}\,[\alpha_1, \cdots, \alpha_{N_s}]$ is a diagonal matrix with diagonal elements given by the channel path gain α_i.

Combining K received signals and assuming the channel matrix $\mathbf{H}$ is time-invariant over the K time instants, we have

$$\mathbf{Y} = [\mathbf{y}_1, \mathbf{y}_2, \cdots, \mathbf{y}_K] = \mathbf{A}_{\text{BS}}(\boldsymbol{\theta})\mathbf{H}_a\mathbf{A}_{\text{MS}}^H(\boldsymbol{\phi})\mathbf{S} + \mathbf{V}, \tag{4}$$

where $\mathbf{S} = [\mathbf{s}_1, \cdots, \mathbf{s}_K]$ and $\mathbf{V} = [\mathbf{v}_1, \cdots, \mathbf{v}_K]$. With $\text{vec}(\mathbf{ABC}) = (\mathbf{C}^T \otimes \mathbf{A})\,\text{vec}(\mathbf{B})$, we can vectorize the received signal matrix as

$$\begin{aligned}\mathbf{y} =& \text{vec}(\mathbf{Y}) = \text{vec}\left(\mathbf{A}_{\text{BS}}(\boldsymbol{\theta})\mathbf{H}_a\mathbf{A}_{\text{MS}}^H(\boldsymbol{\phi})\mathbf{S}\right) + \mathbf{v} \\ =& \left[\left(\mathbf{S}^T\mathbf{A}_{\text{MS}}^*(\boldsymbol{\phi})\right) \otimes \mathbf{A}_{\text{BS}}(\boldsymbol{\theta})\right]\mathbf{h} + \mathbf{v} \triangleq \mathbf{A}(\boldsymbol{\phi}, \boldsymbol{\theta})\mathbf{h} + \mathbf{v}\end{aligned} \tag{5}$$

where $\mathbf{h} = \text{vec}(\mathbf{H}_a) = [\alpha_1\mathbf{e}_1^T, \cdots, \alpha_{N_s}\mathbf{e}_{N_s}^T]^T$ with $\mathbf{e}_i$ denoting an $N_s \times 1$ vector with 1 at the i-th element and 0 elsewhere. It is seen from (5) that the matrix $\mathbf{A}(\boldsymbol{\phi}, \boldsymbol{\theta})$ includes the angle parameters, i.e., the AoDs ϕ_i and AoAs θ_i, and the pilot signals $\mathbf{S}$, while the structural vector $\mathbf{h}$ includes the complex channel path gain α_i.

3. ONE-BIT MASSIVE MIMO SYSTEMS

The use of low-resolution ADCs (e.g., 1-3 bits) for massive MIMO systems has been considered to reduce the hardware complexity and power consumption. In the extreme case of one-bit, the ADC simply compares the input analog signal with a threshold and, hence, requires minimum cost and power consumption.

At each antenna, the in-phase (I) and quadrature (Q) components of the baseband analog signal are quantized separately with a pair of one-bit ADCs. First, we rewrite the complex-valued baseband analog signal at the BS in the real-valued form

$$\bar{\mathbf{y}} = \begin{bmatrix}\mathbf{y}_R \\ \mathbf{y}_I\end{bmatrix} = \bar{\mathbf{A}}(\boldsymbol{\phi}, \boldsymbol{\theta})\bar{\mathbf{h}} + \bar{\mathbf{v}} \tag{6}$$

where

$$\bar{\mathbf{A}} = \begin{bmatrix}\mathbf{A}_R & -\mathbf{A}_I \\ \mathbf{A}_I & \mathbf{A}_R\end{bmatrix}, \quad \bar{\mathbf{h}} = \begin{bmatrix}\mathbf{h}_R \\ \mathbf{h}_I\end{bmatrix}, \quad \text{and } \bar{\mathbf{v}} = \begin{bmatrix}\mathbf{v}_R \\ \mathbf{v}_I\end{bmatrix}.$$

with $\mathbf{X}_R \triangleq \Re\{\mathbf{X}\}$ and $\mathbf{X}_I \triangleq \Im\{\mathbf{X}\}$ denoting the real and imaginary parts of $\mathbf{X}$. Note that the real-valued noise is distributed as $\bar{\mathbf{v}} \sim \mathcal{N}(\mathbf{0}, \frac{\sigma^2}{2}\mathbf{I}_{2KN_r})$. Since the real component is independent of the imaginary component, we can rewrite (6) as

$$\mathbf{y}_R = \mathbf{A}_R\mathbf{h}_R - \mathbf{A}_I\mathbf{h}_I + \mathbf{v}_R \tag{7a}$$

$$\mathbf{y}_I = \mathbf{A}_I\mathbf{h}_R + \mathbf{A}_R\mathbf{h}_I + \mathbf{v}_I \tag{7b}$$

where $\mathbf{v}_R \sim \mathcal{N}(\mathbf{0}, \frac{\sigma^2}{2}\mathbf{I}_{KN_r})$ and $\mathbf{v}_I \sim \mathcal{N}(\mathbf{0}, \frac{\sigma^2}{2}\mathbf{I}_{KN_r})$.

Then, the one-bit quantized output of the received signal is

$$\mathbf{z}_R = \text{sign}(\mathbf{y}_R - \boldsymbol{\lambda}_R), \tag{8a}$$

$$\mathbf{z}_I = \text{sign}(\mathbf{y}_I - \boldsymbol{\lambda}_I), \tag{8b}$$

where $\boldsymbol{\lambda}_R \in \mathbb{R}^{KN_r \times 1}$ and $\boldsymbol{\lambda}_I \in \mathbb{R}^{KN_r \times 1}$ denote, respectively, the thresholds used at the I and Q channels for all N_r antennas across K pilot signals.

4. CRAMÉR-RAO BOUNDS ON ONE-BIT MASSIVE MIMO CHANNEL ESTIMATION

The problem of interest here is to estimate the angular AoDs ($\boldsymbol{\theta}$) and AoAs ($\boldsymbol{\phi}$), as well as the associated channel path gains $\boldsymbol{\alpha}$ from the quantized signal $\mathbf{z} = [\mathbf{z}_R^T, \mathbf{z}_I^T]^T$. In the following, we derive the performance bound in terms of the CRBs for any unbiased estimator of these unknown parameters.

First group all unknown real-valued parameters as

$$\boldsymbol{\psi} = [\boldsymbol{\theta}^T, \boldsymbol{\phi}^T, \boldsymbol{\alpha}_R^T, \boldsymbol{\alpha}_I^T, \sigma^2]^T, \tag{9}$$

where $\boldsymbol{\alpha}_R = \Re\{\boldsymbol{\alpha}\}$ and $\boldsymbol{\alpha}_I = \Im\{\boldsymbol{\alpha}\}$. Invoking the independence across K time instants and between the real and imaginary components, the joint log-likelihood function of $\mathbf{z}$ can be expressed as

$$\ln p(\mathbf{z}|\boldsymbol{\psi}) = \sum_{m=1}^{KN_r} \left[\ln \Phi\left(z_R(m)\eta_m\right) + \ln \Phi\left(z_I(m)\zeta_m\right)\right], \tag{10}$$

where

$$\eta_m = \frac{\mathbf{A}_R^T(m)\mathbf{h}_R - \mathbf{A}_I^T(m)\mathbf{h}_I - \lambda_R(m)}{\sigma/\sqrt{2}}, \tag{11a}$$

$$\zeta_m = \frac{\mathbf{A}_I^T(m)\mathbf{h}_R + \mathbf{A}_R^T(m)\mathbf{h}_I - \lambda_I(m)}{\sigma/\sqrt{2}}, \tag{11b}$$

$\Phi(\cdot)$ is the cumulative density function (CDF) of a standard normal random variable, $z_{R/I}(m)$ is the m-th element of $\mathbf{z}_{R/I}$, $\mathbf{A}_{R/I}^T(m)$ denotes the m-th row of $\mathbf{A}_{R/I}$ in (6), and we ignore their dependence on $\boldsymbol{\phi}$ and $\boldsymbol{\theta}$ for brevity. With the joint log-likelihood function of $\mathbf{z}$, the general expression of each element of FIM is given by

$$\mathbf{F}_{p,q}(\boldsymbol{\psi}) = -E\left\{\frac{\partial^2 \ln p(\mathbf{z}|\boldsymbol{\psi})}{\partial\psi_p\partial\psi_q}\right\}. \tag{12}$$

where $p, q \in \{1, 2, \cdots, 4N_s + 1\}$ and

$$\mathbf{F}(\boldsymbol{\psi}) = \begin{bmatrix}\mathbf{F}_{A,A}(\boldsymbol{\psi}) & \mathbf{F}_{A,\sigma^2}(\boldsymbol{\psi}) \\ \mathbf{F}_{A,\sigma^2}^T(\boldsymbol{\psi}) & F_{\sigma^2,\sigma^2}(\boldsymbol{\psi})\end{bmatrix} \in \mathbb{R}^{(4N_s+1)\times(4N_s+1)} \tag{13}$$

where $\mathbf{F}_{A,A}(\boldsymbol{\psi})$ is the FIM block for the angle parameters

$$\mathbf{F}_{A,A}(\boldsymbol{\psi}) = \begin{bmatrix} \mathbf{F}_{\boldsymbol{\theta},\boldsymbol{\theta}} & \mathbf{F}_{\boldsymbol{\theta},\boldsymbol{\phi}} & \mathbf{F}_{\boldsymbol{\theta},\boldsymbol{\alpha}_R} & \mathbf{F}_{\boldsymbol{\theta},\boldsymbol{\alpha}_I} \\ \mathbf{F}_{\boldsymbol{\theta},\boldsymbol{\phi}}^T & \mathbf{F}_{\boldsymbol{\phi},\boldsymbol{\phi}} & \mathbf{F}_{\boldsymbol{\phi},\boldsymbol{\alpha}_R} & \mathbf{F}_{\boldsymbol{\phi},\boldsymbol{\alpha}_I} \\ \mathbf{F}_{\boldsymbol{\theta},\boldsymbol{\alpha}_R}^T & \mathbf{F}_{\boldsymbol{\phi},\boldsymbol{\alpha}_R}^T & \mathbf{F}_{\boldsymbol{\alpha}_R,\boldsymbol{\alpha}_R} & \mathbf{F}_{\boldsymbol{\alpha}_R,\boldsymbol{\alpha}_I} \\ \mathbf{F}_{\boldsymbol{\theta},\boldsymbol{\alpha}_I}^T & \mathbf{F}_{\boldsymbol{\phi},\boldsymbol{\alpha}_I}^T & \mathbf{F}_{\boldsymbol{\alpha}_R,\boldsymbol{\alpha}_I}^T & \mathbf{F}_{\boldsymbol{\alpha}_I,\boldsymbol{\alpha}_I} \end{bmatrix}. \quad (14)$$

For any unbiased estimator of $\boldsymbol{\psi}$, the CRB provides a lower bound on the estimation variance

$$\text{cov}(\hat{\psi}_p) \geq \left[\mathbf{F}^{-1}(\boldsymbol{\psi})\right]_{p,p}, \quad (15)$$

where $\mathbf{F}(\boldsymbol{\psi})$ is the complete FIM given by (13). With (10), we are ready to derive the FIM in (13) and establish the performance bounds on the estimation of all unknown parameters $\boldsymbol{\psi}$.

4.1. General Expressions for Fisher Information Matrix

Note that

$$E\left\{\frac{1}{\Phi^2\left(z_R(m)\eta_m\right)}\right\} = \frac{1}{\Phi\left(\eta_m\right)} + \frac{1}{\Phi\left(-\eta_m\right)}, \quad (19)$$

$$E\left\{\frac{1}{\Phi^2\left(z_I(m)\zeta_m\right)}\right\} = \frac{1}{\Phi\left(\zeta_m\right)} + \frac{1}{\Phi\left(-\zeta_m\right)}. \quad (20)$$

Taking the expectation over the second derivatives of the log-likelihood function and invoking the independence over k and I/Q components yield the general expressions of FIM shown in (16) for $\mathbf{F}_{A,A}(\boldsymbol{\psi})$, (17) for $\mathbf{F}_{A,\sigma^2}(\boldsymbol{\psi})$, and (18) for $\mathbf{F}_{\sigma^2,\sigma^2}(\boldsymbol{\psi})$, where $\partial\mathbf{A}_R^T(m)/\partial\theta_i$ is the m-th row of $\partial\mathbf{A}_R/\partial\theta_i$. To compute (16), (17) and (18), we still need to compute the following partial derivatives: $\partial\mathbf{A}_R^T(m)/\partial\theta_i$, $\partial\mathbf{A}_I^T(m)/\partial\theta_i$, $\partial\mathbf{A}_R^T(m)/\partial\phi_i$, $\partial\mathbf{A}_I^T(m)/\partial\phi_i$, $\partial\mathbf{h}_R/\partial\alpha_{R,i}$ and $\partial\mathbf{h}_I/\partial\alpha_{I,i}$.

4.2. Partial Derivatives for Fisher Information Matrix

Given that $\mathbf{A} = \left(\mathbf{S}^T\mathbf{A}_{\text{MS}}^*(\boldsymbol{\phi})\right) \otimes \mathbf{A}_{\text{BS}}(\boldsymbol{\theta})$, we have

$$\mathbf{A}_R = \left(\mathbf{S}_R^T\mathbf{A}_{\text{MS}}^R + \mathbf{S}_I^T\mathbf{A}_{\text{MS}}^I\right) \otimes \mathbf{A}_{\text{BS}}^R - \left(\mathbf{S}_I^T\mathbf{A}_{\text{MS}}^R - \mathbf{S}_R^T\mathbf{A}_{\text{MS}}^I\right) \otimes \mathbf{A}_{\text{BS}}^I,$$

$$\mathbf{A}_I = \left(\mathbf{S}_R^T\mathbf{A}_{\text{MS}}^R + \mathbf{S}_I^T\mathbf{A}_{\text{MS}}^I\right) \otimes \mathbf{A}_{\text{BS}}^I + \left(\mathbf{S}_I^T\mathbf{A}_{\text{MS}}^R - \mathbf{S}_R^T\mathbf{A}_{\text{MS}}^I\right) \otimes \mathbf{A}_{\text{BS}}^R,$$

where the sub-index and super-index (I/R) indicate the real or imaginary part of the corresponding matrix. Similarly, we have $\mathbf{h}_R = [\alpha_{R,1}\mathbf{e}_1^T, \cdots, \alpha_{R,N_s}\mathbf{e}_{N_s}^T]^T$ and $\mathbf{h}_I = [\alpha_{I,1}\mathbf{e}_1^T, \cdots, \alpha_{I,N_s}\mathbf{e}_{N_s}^T]^T$.

First, we derive the partial derivatives of $\mathbf{A}_R$ and $\mathbf{A}_I$ w.r.t. the AoA and AoD

$$\frac{\partial\mathbf{A}_R}{\partial\theta_i} = (\mathbf{S}_R^T\mathbf{A}_{\text{MS}}^R + \mathbf{S}_I^T\mathbf{A}_{\text{MS}}^I) \otimes \frac{\partial\mathbf{A}_{\text{BS}}^R}{\partial\theta_i} - (\mathbf{S}_I^T\mathbf{A}_{\text{MS}}^R - \mathbf{S}_R^T\mathbf{A}_{\text{MS}}^I) \otimes \frac{\partial\mathbf{A}_{\text{BS}}^I}{\partial\theta_i}, \quad (21)$$

$$\frac{\partial\mathbf{A}_I}{\partial\theta_i} = (\mathbf{S}_R^T\mathbf{A}_{\text{MS}}^R + \mathbf{S}_I^T\mathbf{A}_{\text{MS}}^I) \otimes \frac{\partial\mathbf{A}_{\text{BS}}^I}{\partial\theta_i} + (\mathbf{S}_I^T\mathbf{A}_{\text{MS}}^R - \mathbf{S}_R^T\mathbf{A}_{\text{MS}}^I) \otimes \frac{\partial\mathbf{A}_{\text{BS}}^R}{\partial\theta_i}, \quad (22)$$

$$\frac{\partial\mathbf{A}_R}{\partial\phi_i} = (\mathbf{S}_R^T\frac{\partial\mathbf{A}_{\text{MS}}^R}{\partial\phi_i} + \mathbf{S}_I^T\frac{\partial\mathbf{A}_{\text{MS}}^I}{\partial\phi_i}) \otimes \mathbf{A}_{\text{BS}}^R - (\mathbf{S}_I^T\frac{\partial\mathbf{A}_{\text{MS}}^R}{\partial\phi_i} - \mathbf{S}_R^T\frac{\partial\mathbf{A}_{\text{MS}}^I}{\partial\phi_i}) \otimes \mathbf{A}_{\text{BS}}^I, \quad (23)$$

$$\frac{\partial\mathbf{A}_I}{\partial\phi_i} = (\mathbf{S}_R^T\frac{\partial\mathbf{A}_{\text{MS}}^R}{\partial\phi_i} + \mathbf{S}_I^T\frac{\partial\mathbf{A}_{\text{MS}}^I}{\partial\phi_i}) \otimes \mathbf{A}_{\text{BS}}^I + (\mathbf{S}_I^T\frac{\partial\mathbf{A}_{\text{MS}}^R}{\partial\phi_i} - \mathbf{S}_R^T\frac{\partial\mathbf{A}_{\text{MS}}^I}{\partial\phi_i}) \otimes \mathbf{A}_{\text{BS}}^R. \quad (24)$$

In the case of ULA, we have

$$\frac{\partial\mathbf{A}_{\text{BS}}^{R/I}}{\partial\theta_i} = [\mathbf{0}_{N_r\times(i-1)}, \overset{\prime}{\mathbf{a}}_{\text{BS},R/I}(\theta_i), \mathbf{0}_{N_r\times(Ns-i)}],$$

$$\frac{\partial\mathbf{A}_{\text{MS}}^{R/I}}{\partial\phi_i} = [\mathbf{0}_{N_r\times(i-1)}, \overset{\prime}{\mathbf{a}}_{\text{MS},R/I}(\phi_i), \mathbf{0}_{N_r\times(Ns-i)}],$$

where

$$\overset{\prime}{\mathbf{a}}_{\text{BS},R}(\theta_i) = \frac{-2\pi d_r}{\lambda\sqrt{N_r}}\left[0, \cdots, (N_r-1)\sin\left(\frac{(N_r-1)2\pi d_r\sin(\theta_i)}{\lambda}\right)\cos(\theta_i)\right]^T,$$

$$\overset{\prime}{\mathbf{a}}_{\text{BS},I}(\theta_i) = \frac{-2\pi d_r}{\lambda\sqrt{N_r}}\left[0, \cdots, (N_r-1)\cos\left(\frac{(N_r-1)2\pi d_r\sin(\theta_i)}{\lambda}\right)\cos(\theta_i)\right]^T,$$

$$\overset{\prime}{\mathbf{a}}_{\text{MS},R}(\phi_i) = \frac{-2\pi d_t}{\lambda\sqrt{N_t}}\left[0, \cdots, (N_t-1)\sin\left(\frac{(N_t-1)2\pi d_t\sin(\phi_i)}{\lambda}\right)\cos(\phi_i)\right]^T,$$

$$\overset{\prime}{\mathbf{a}}_{\text{MS},I}(\phi_i) = \frac{2\pi d_t}{\lambda\sqrt{N_t}}\left[0, \cdots, (N_t-1)\cos\left(\frac{(N_t-1)2\pi d_t\sin(\phi_i)}{\lambda}\right)\cos(\phi_i)\right]^T.$$

The partial derivatives of $\mathbf{h}_R$ and $\mathbf{h}_I$ w.r.t. $\alpha_{R,i}$ and $\alpha_{I,i}$ are given as

$$\frac{\partial\mathbf{h}_R}{\partial\alpha_{R,i}} = [\underbrace{\mathbf{0}_{N_s}^T, \cdots, \mathbf{0}_{N_s}^T}_{i-1 \text{ zero vectors}}, \mathbf{e}_i^T, \mathbf{0}_{N_s}^T, \cdots, \mathbf{0}_{N_s}^T]^T, \quad (25)$$

$$\frac{\partial\mathbf{h}_I}{\partial\alpha_{I,i}} = [\underbrace{\mathbf{0}_{N_s}^T, \cdots, \mathbf{0}_{N_s}^T}_{i-1 \text{ zero vectors}}, \mathbf{e}_i^T, \mathbf{0}_{N_s}^T, \cdots, \mathbf{0}_{N_s}^T]^T. \quad (26)$$

With (21), (22), (23), (24) and (25), (26), we obtain all partial derivatives to compute the FIM elemenets of (13) via (16), (17), and (18).

4.3. Observations on CRBs

The following observations on the derived CRB are in order.

- For a clairvoyant quantization scheme (denoted as CQ) with $\boldsymbol{\lambda} = \boldsymbol{\Gamma}(\boldsymbol{\phi},\boldsymbol{\theta})\bar{\mathbf{h}}$ when the noise variance σ^2 is unknown, the corresponding FIM $\mathbf{F}(\boldsymbol{\psi})$ of (13) is *singular* since $\mathbf{F}_{A,\sigma^2}(\boldsymbol{\psi})$ and $F_{\sigma^2,\sigma^2}(\boldsymbol{\psi})$, defined by (17) and (18), respectively, become zeros.

- For a fixed zero-threshold quantization scheme (denoted as FQ) (i.e., $\lambda = 0$) when σ^2 is unknown, the corresponding FIM of (13) is also *singular* due to an ambiguity between the amplitude $\mathbf{h}$ and the noise variance σ^2. It can be seen that, for given one-bit measurements $\mathbf{z}_R$ and $\mathbf{z}_I$, two pairs of $[\mathbf{h}, \sigma^2]$ and $[s\mathbf{h}, (s\sigma)^2]$ give the same η_m and ζ_m of (11) and, hence, the same likelihood function of (10), where s is a scalar. This ambiguity is removed if a fixed non-zero threshold is used and the corresponding FIM becomes *non-singular*.

- When the noise variance σ^2 is known, the unknown parameter set reduces to $\boldsymbol{\psi} = [\boldsymbol{\theta}^T, \boldsymbol{\phi}^T, \boldsymbol{\alpha}_R^T, \boldsymbol{\alpha}_I^T]^T$ and the FIM reduces to $\mathbf{F}_{A,A}(\boldsymbol{\psi})$ of (14). The CRB with known noise variance is, therefore, $\text{cov}(\hat{\psi}_p) \geq \left[\mathbf{F}_{A,A}^{-1}(\boldsymbol{\psi})\right]_{p,p}$. In this case, the FIMs for the FQ and CQ are both *non-singular*.

- We also consider a time-varying threshold quantization (denoted as TQ) scheme [23, 24], originally proposed for the (sparse) spectrum analysis, for one-bit massive MIMO channel estimation. For a given time instant, the TQ randomly selects a threshold according to a probability distribution (e.g., the discrete uniform distribution) from a pre-defined set $[-h_{\max}, -h_{\max}+\Delta, \cdots, 0, \cdots, h_{\max}-\Delta, h_{\max}]$, where $h_{\max}$ is the dynamic range and Δ is the stepsize. For the TQ scheme, the FIM is *non-singular* with a high probability for known and unknown noise variances. It is interesting to note that the CQ scheme can be considered as a special case of the TQ scheme, which leads to a singular FIM.

$$[\mathbf{F}_{A,A}(\boldsymbol{\psi})]_{p,q} = \frac{1}{\pi\sigma^2}\sum_{m=1}^{KN_r}\left[\left(\frac{1}{\Phi(\eta_m)}+\frac{1}{\Phi(-\eta_m)}\right)e^{-\eta_m^2}\frac{\partial\left(\mathbf{A}_R^T(m)\mathbf{h}_R-\mathbf{A}_I^T(m)\mathbf{h}_I\right)}{\partial\psi_p}\frac{\partial\left(\mathbf{A}_R^T(m)\mathbf{h}_R-\mathbf{A}_I^T(m)\mathbf{h}_I\right)}{\partial\psi_q}\right.$$
$$\left.+\left(\frac{1}{\Phi(\zeta_m)}+\frac{1}{\Phi(-\zeta_m)}\right)e^{-\zeta_m^2}\frac{\partial\left(\mathbf{A}_I^T(m)\mathbf{h}_R+\mathbf{A}_R^T(m)\mathbf{h}_I\right)}{\partial\psi_p}\frac{\partial\left(\mathbf{A}_I^T(m)\mathbf{h}_R+\mathbf{A}_R^T(m)\mathbf{h}_I\right)}{\partial\psi_q}\right], 1\le p,q\le 4N_s, \quad (16)$$

$$[\mathbf{F}_{A,\sigma^2}(\boldsymbol{\psi})]_p = -\frac{1}{2\pi\sigma^4}\sum_{m=1}^{KN_r}\left[\left(\frac{1}{\Phi(\eta_m)}+\frac{1}{\Phi(-\eta_m)}\right)e^{-\eta_m^2}\frac{\partial\left(\mathbf{A}_R^T(m)\mathbf{h}_R-\mathbf{A}_I^T(m)\mathbf{h}_I\right)}{\partial\psi_p}\left(\mathbf{A}_R^T(m)\mathbf{h}_R-\mathbf{A}_I^T(m)\mathbf{h}_I-\lambda_R(m)\right)\right.$$
$$\left.+\left(\frac{1}{\Phi(\zeta_m)}+\frac{1}{\Phi(-\zeta_m)}\right)e^{-\zeta_m^2}\frac{\partial\left(\mathbf{A}_I^T(m)\mathbf{h}_R+\mathbf{A}_R^T(m)\mathbf{h}_I\right)}{\partial\psi_p}\left(\mathbf{A}_I^T(m)\mathbf{h}_R+\mathbf{A}_R^T(m)\mathbf{h}_I-\lambda_I(m)\right)\right], \quad (17)$$

$$F_{\sigma^2,\sigma^2}(\boldsymbol{\psi}) = \frac{1}{4\pi\sigma^6}\sum_{m=1}^{KN_r}\left[\left(\frac{1}{\Phi(\eta_m)}+\frac{1}{\Phi(-\eta_m)}\right)e^{-\eta_m^2}\left(\mathbf{A}_R^T(m)\mathbf{h}_R-\mathbf{A}_I^T(m)\mathbf{h}_I-\lambda_R(m)\right)^2\right.$$
$$\left.+\left(\frac{1}{\Phi(\zeta_m)}+\frac{1}{\Phi(-\zeta_m)}\right)e^{-\zeta_m^2}\left(\mathbf{A}_I^T(m)\mathbf{h}_R+\mathbf{A}_R^T(m)\mathbf{h}_I-\lambda_I(m)\right)^2\right]. \quad (18)$$

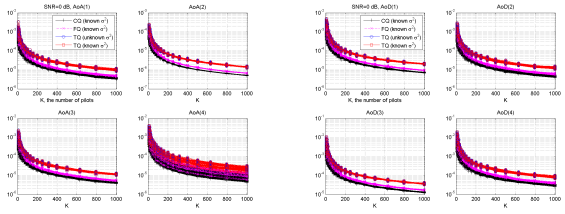

(a) AoA (b) AoD

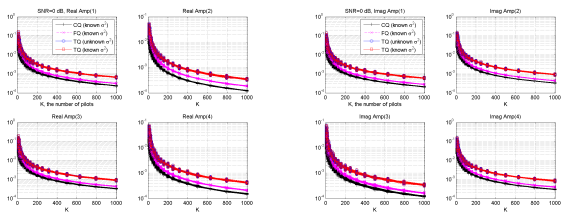

(c) Path gain (real) (d) Path gain (imaginary)

Fig. 2. CRB comparison as a function of K when SNR $= 0$ dB.

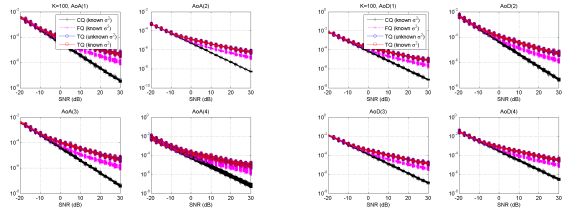

(a) AoA (b) AoD

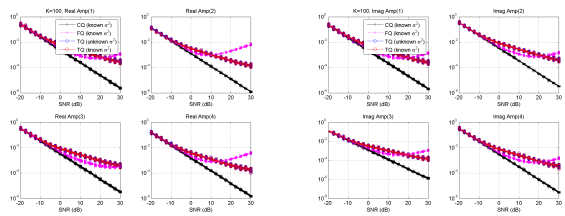

(c) Path gain (real) (d) Path gain (imaginary)

Fig. 3. CRB comparisons as a function of SNR when $K = 100$.

5. NUMERICAL RESULTS

We now provide simulation results to compare channel estimation performance among several one-bit quantization schemes[1]. In particular, we consider 1) the CQ scheme (i.e., $\boldsymbol{\lambda} = \boldsymbol{\Gamma}(\boldsymbol{\phi},\boldsymbol{\theta})\bar{\mathbf{h}}$) with *known* noise variance; 2) the zero-threhold FQ scheme (i.e., $\boldsymbol{\lambda} = \mathbf{0}$) with *known* noise variance; 3) the TQ scheme with either known or unknown noise variance [23,24]. It uses the discrete uniform distribution to select the threshold at a given time instant.

We consider a system model consisting of 8 ULA antennas at the MS and 16 ULA antennas at the BS. The wireless MIMO channel is assumed to follow a geometric model of $N_s = 4$ scatterers with each of AoAs and AoDs from the following 4 clusters:

- $\text{AoD}_1 = [15°, 18°]$ and $\text{AoA}_1 = [-50°, -45°]$;
- $\text{AoD}_2 = [45°, 50°]$ and $\text{AoA}_2 = [-10°, -5°]$;
- $\text{AoD}_3 = [-20°, -16°]$ and $\text{AoA}_3 = [30°, 36°]$;
- $\text{AoD}_4 = [-72°, -70°]$ and $\text{AoA}_4 = [65°, 75°]$.

[1]The MATLAB code is available at www.merl.com to compute the derived CRB for known and unknown noise variances.

First, we compare the CRBs as a function of the number of pilots K when SNR $= 0$ dB. Specifically, the SNR is defined on a per receive antenna basis, i.e., SNR $= \|\mathbf{A}(\boldsymbol{\phi},\boldsymbol{\theta})\mathbf{h}\|^2/(KN_r\sigma^2)$. Since the CRB depends on channel parameters, thresholds, and pilot signals, we run 100 independent Monte-Carlo simulations. For each Monte-Carlo run, the four pairs of AoA ($\boldsymbol{\theta}$) and AoD ($\boldsymbol{\phi}$) are randomly drawn from the above clusters. The pilot signal ($\mathbf{S}$) and the four channel path gain ($\boldsymbol{\alpha}$) are randomly generated once and then fixed throughout Monte-Carlo runs. Fig. 2 shows 100 CRB curves for the one-bit quantization schemes considered for each of the four channel parameters of AoA, AoD, the real and imaginary parts of the channel path gain. For the TQ scheme, we further average the CRB over uniformly drawn thresholds from 8 evenly spaced levels in $[-h_{\max}, h_{\max}]$ with $h_{\max} = \max\{\boldsymbol{\Gamma}(\boldsymbol{\phi},\boldsymbol{\theta})\bar{\mathbf{h}}\}$. It is seen that the CQ scheme with known σ^2 provides the lower bounds for the one-bit channel estimation performance, while the FQ with known σ^2 gives slightly worse CRB curves. On the other hand, the TQ scheme gives very close CRB curves when the noise variance σ^2 is known and unknown. Overall, the CRBs for estimating angle parameters (i.e., AoA and AoD) are lower than those for estimating path gains.

Second, we compare the CRBs as a function of SNR when

$K = 100$. Fig. 3 shows 100 CRB curves for the one-bit quantization schemes considered. It is seen that, for the CQ scheme with known σ^2, its CRB is log-linear with respect to the SNR in the dB scale, while the CRBs deviate from the log-linear curve at high SNRs for the FQ and TQ schemes, as the quantization error dominates the additive noise. It is interesting to see that the TQ scheme gives lower CRB curves for the channel path gains than the zero-threshold FQ scheme with known σ^2 at high SNRs.

6. CONCLUSION

This paper has considered the CRB for estimating the angular-domain channel parameters, such as the angle-of-departure, angle-of-arrival and associated channel path gains, for massive MIMO systems with one-bit ADCs. By evaluating several one-bit quantization schemes, the derived CRB provides a simple tool to compare their channel estimation performance. The numerical comparison clearly shows the advantage of the time-varying one-bit quantization scheme for estimating the channel path gains.

7. REFERENCES

[1] T. L. Marzetta, "Noncooperative cellular wireless with unlimited numbers of base station antennas," *IEEE Trans. on Wireless Communications*, vol. 9, no. 11, pp. 3590–3600, November 2010.

[2] F. Rusek, D. Persson, B. K. Lau, E. G. Larsson, T. L. Marzetta, O. Edfors, and F. Tufvesson, "Scaling up MIMO: Opportunities and challenges with very large arrays," *IEEE Signal Processing Magazine*, vol. 30, no. 1, pp. 40–60, Jan 2013.

[3] E. G. Larsson, O. Edfors, F. Tufvesson, and T. L. Marzetta, "Massive MIMO for next generation wireless systems," *IEEE Communications Magazine*, vol. 52, no. 2, pp. 186–195, February 2014.

[4] T. S. Rappaport et. al., "Millimeter wave mobile communications for 5G cellular: It will work!," *IEEE Access*, vol. 1, pp. 335–349, 2013.

[5] S. Rangan, T. S. Rappaport, and E. Erkip, "Millimeter-wave cellular wireless networks: Potentials and challenges," *Proceedings of the IEEE*, vol. 102, no. 3, pp. 366–385, March 2014.

[6] M. R. Akdeniz et. al., "Millimeter wave channel modeling and cellular capacity evaluation," *IEEE Journal on Selected Areas in Communications*, vol. 32, no. 6, pp. 1164–1179, June 2014.

[7] P. Wang, M. Pajovic, P. V. Orlik, T. Koike-Akino, K. J. Kim, and J. Fang, "Sparse channel estimation in millimeter wave communications: Exploiting joint AoD-AoA angular spread," in *2017 IEEE International Conference on Communications (ICC)*, May 2017, pp. 1–6.

[8] A. L. Swindlehurst, E. Ayanoglu, P. Heydari, and F. Capolino, "Millimeter-wave massive MIMO: the next wireless revolution," *IEEE Commun. Mag.*, vol. 52, no. 9, pp. 56–62, September 2014.

[9] B. Ai, K. Guan, R. He, J. Li, G. Li, D. He, Z. Zhong, and K. M. S. Huq, "On indoor millimeter wave massive MIMO channels: Measurement and simulation," *IEEE Journal on Selected Areas in Communications*, vol. 35, no. 7, pp. 1678–1690, July 2017.

[10] J. Wang, "Beam codebook based beamforming protocol for multi-Gbps millimeter-wave WPAN systems," *IEEE Journal on Selected Areas in Communications*, vol. 27, no. 8, pp. 1390–1399, October 2009.

[11] S. Hur, T. Kim, D. J. Love, J. V. Krogmeier, T. A. Thomas, and A. Ghosh, "Millimeter wave beamforming for wireless backhaul and access in small cell networks," *IEEE Transactions on Communications*, vol. 61, no. 10, pp. 4391–4403, October 2013.

[12] A. Alkhateeb, O. E. Ayach, G. Leus, and R. W. Heath, "Channel estimation and hybrid precoding for millimeter wave cellular systems," *IEEE Journal of Selected Topics in Signal Processing*, vol. 8, no. 5, pp. 831–846, October 2014.

[13] S. Han, C. l. I, Z. Xu, and C. Rowell, "Large-scale antenna systems with hybrid analog and digital beamforming for millimeter wave 5G," *IEEE Communications Magazine*, vol. 53, no. 1, pp. 186–194, January 2015.

[14] R. Méndez-Rial, C. Rusu, N. Gonzlez-Prelcic, A. Alkhateeb, and R. W. Heath, "Hybrid MIMO architectures for millimeter wave communications: Phase shifters or switches?," *IEEE Access*, vol. 4, pp. 247–267, 2016.

[15] C. Risi, D. Persson, and E. G. Larsson, "Massive MIMO with 1-bit ADC," *arXiv preprint*, vol. arXiv:1404.7736, 2014.

[16] L. Fan, S. Jin, C.-K. Wen, and H. Zhang, "Uplink achievable rate for massive MIMO systems with low-resolution ADC," *IEEE Commun. Lett.*, vol. 19, no. 12, pp. 2186–2189, 2015.

[17] J. Zhang, L. Dai, S. Sun, and Z. Wang, "On the spectral efficiency of massive MIMO systems with low-resolution ADCs," *IEEE Commun. Lett.*, vol. 20, no. 5, pp. 842–845, 2016.

[18] S. Wang, Y. Li, and J. Wang, "Multiuser detection in massive spatial modulation MIMO with low-resolution ADCs," *IEEE Trans. Wireless Commun.*, vol. 14, no. 4, pp. 2156–2168, 2015.

[19] C.-K. Wen, C.-J. Wang, S. Jin, K.-K. Wong, and P. Ting, "Bayes-optimal joint channel-and-data estimation for massive MIMO with low-precision ADCs," *IEEE Trans. Signal Process.*, vol. 64, no. 10, pp. 2541–2556, 2016.

[20] J. Choi, J. Mo, and R. W. Heath, "Near maximum-likelihood detector and channel estimator for uplink multiuser massive MIMO systems with one-bit ADCs," *IEEE Trans. Commun.*, vol. 64, no. 5, pp. 2005–2018, 2016.

[21] J. Mo and R. W. Heath, "Capacity analysis of one-bit quantized MIMO systems with transmitter channel state information," *IEEE Trans. Signal Process.*, vol. 63, no. 20, pp. 5498–5512, 2015.

[22] J. Mo, P. Schniter, N. G. Prelcic, and R. W. Heath, "Channel estimation in millimeter wave MIMO systems with one-bit quantization," in *2014 48th Asilomar Conference on Signals, Systems and Computers*, Nov 2014, pp. 957–961.

[23] C. Gianelli, L. Xu, J. Li, and P. Stoica, "One-bit compressive sampling with time-varying thresholds: Maximum likelihood and the cramer-rao bound," in *2016 50th Asilomar Conference on Signals, Systems and Computers*, Nov 2016, pp. 399–403.

[24] C. Gianelli, L. Xu, J. Li, and P. Stoica, "One-bit compressive sampling with time-varying thresholds for sparse parameter estimation," in *2016 IEEE Sensor Array and Multichannel Signal Processing Workshop (SAM)*, July 2016, pp. 1–5.